Self-consistent-field calculations of proteinlike incorporations in polyelectrolyte complex micelles

Saskia Lindhoud,[1,*] Martien A. Cohen Stuart,[1] Willem Norde,[1,2] and Frans A. M. Leermakers[1]
[1]*Laboratory of Physical Chemistry and Colloid Science, Wageningen University, Dreijenplein 6, 6703 HB Wageningen, The Netherlands*
[2]*Department of Biomedical Engineering, University Medical Center Groningen and University of Groningen, A. Deusinglaan 1, 9713 AV Groningen, The Netherlands*
(Received 29 July 2009; published 24 November 2009)

Self-consistent field theory is applied to model the structure and stability of polyelectrolyte complex micelles with incorporated protein (molten globule) molecules in the core. The electrostatic interactions that drive the micelle formation are mimicked by nearest-neighbor interactions using Flory-Huggins χ parameters. The strong qualitative comparison with experimental data proves that the Flory-Huggins approach is reasonable. The free energy of insertion of a proteinlike molecule into the micelle is nonmonotonic: there is (i) a small repulsion when the protein is inside the corona; the height of the insertion barrier is determined by the local osmotic pressure and the elastic deformation of the core, (ii) a local minimum occurs when the protein molecule is at the core-corona interface; the depth (a few k_BT's) is related to the interfacial tension at the core-corona interface and (iii) a steep repulsion (several k_BT) when part of the protein molecule is dragged into the core. Hence, the protein molecules reside preferentially at the core-corona interface and the absorption as well as the release of the protein molecules has annealed rather than quenched characteristics. Upon an increase of the ionic strength it is possible to reach a critical micellization ionic (CMI) strength. With increasing ionic strength the aggregation numbers decrease strongly and only few proteins remain associated with the micelles near the CMI.

DOI: 10.1103/PhysRevE.80.051406 PACS number(s): 82.70.−y, 87.15.nr, 87.15.bk

I. INTRODUCTION

Incorporation of proteins in nanostructures is of interest for food, pharmaceutical, and industrial applications. Polyelectrolyte complex micelles that formed by attractive electrostatic forces between chains with opposite charge [1–3], have successfully been used to incorporate proteins [4–6]. Many proteins have multiple charges at their surface (even near their iso-electric point). These charges provide the proteins with a weak cooperative binding mechanism (much weaker than simple 1:1 electrolyte) to oppositely charged chains that are abundantly present in the core of such micelles. This binding mechanism is generic and may be modified by other nongeneric interactions (specific binding).

To model the electrostatic driving force is a major challenge for state-of-the-art self-consistent field (SCF) modeling, because the core that is composed of two oppositely charged species is in essence electroneutral. In the mean-field SCF theory, the chains in the bulk (i.e., in the reference state) are modeled as quasineutral Gaussian chains, with small ions compensating the charge of the electrolyte chains. When such chains are forced to pack in an electroneutral core, they again do not feel electrostatic interactions. As a result, on the level of the SCF theory, there is no driving force for the assembly. The attractive force between plus and minus (requiring ion correlation) is not captured. The high packing density in the core is against the assembly. In the absence of any other attractive forces the micelles should fall apart spontaneously.

Recently, however, it was shown that, to first order, one may replace the electrostatic correlation force by a negative (attractive) Flory-Huggins parameter [7]. It is rather common that the Flory-Huggins parameters are used to account for a complex underlying interaction. For example in alkyl surfactants, the SCF model features a simple χ parameter for the interaction between hydrocarbon segment and water, completely ignoring the H-bonding structure of water and how this is affected by the alkyl segment. In doing so, the SCF model obviously cannot predict temperature dependencies for such systems, but structural features on a micellar level are reasonably accounted for. For the current problem, it is expected that the electrostatic forces inside the core are short ranged, because the electrostatic attraction is only felt locally between nearby positively and negatively charged units and it may hence be reasonable to invoke a short-range parameter to capture this. In doing so, one may, e.g., loose detailed information on entropic and energetic contributions hidden in such an effective parameter, but importantly, one can still use the classical self-consistent field method to obtain relevant structural information.

The particles of interest in this study are interpolyelectrolyte complex micelles [1–3]. These association colloids are formed when a diblock copolymer, having a charged as well as a neutral hydrophilic block, and an oppositely charged macromolecule are mixed at about equal charge ratio. The oppositely charged macromolecules may be diblock copolymers [1,2,8–11], homopolymers [3,12,13], DNA [14,15], and proteins [4–6], etc. The micelles have a core-corona structure: the core consists of the two oppositely charged polyelectrolyte species, the corona is formed by the (uncharged) hydrophilic block(s) of the diblock copolymer(s).

Previous experimental work revealed that, in order to obtain stable micelles with a protein-containing core, one can dilute the core of the micelles with a certain amount of homopolyelectrolyte, which has the same charge sign as the protein [4]. When the ratio between protein molecules and homopolymers is such that the homopolymer is in excess (see Fig. 1), the polyelectrolyte complex micelles persist up

*saskia.lindhoud@wur.nl; saskia.lindhoud@gmail.com

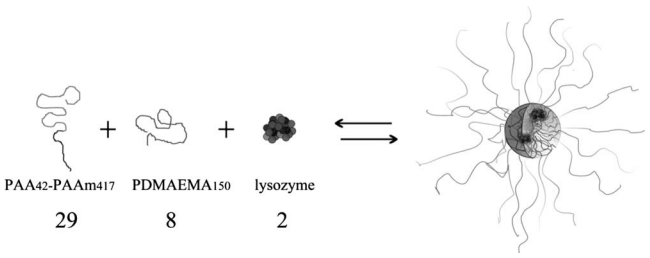

FIG. 1. Artistic impression of the formation of lysozyme-filled polyelectrolyte complex micelles. The numbers indicate the aggregation number of the different components of the lysozyme-filled micelle (derived from SANS data [16]).

to a salt concentration of 0.5 M NaCl. Above this salt concentration the micelles disintegrate due to the screening of the charges within the polyelectrolyte complex core [4]. One of the aims of the theoretical modeling presented here, is to get deeper understanding of the entire co-assembly process as presented in Fig. 1.

Quite generally, micelles form, rather suddenly upon exceeding a certain (polymer) concentration, which is called the "critical micelle concentration" (CMC). The sharpness of this threshold is a consequence of the cooperative character of micelle formation. The equilibrium between free molecules and micelles can be affected by environmental conditions. Classical (surfactant or block copolymer) micelles often have, for a given polymer concentration, a critical micellization temperature (CMT), micelles usually form at $T>\mathrm{CMT}$. For polyelectrolyte complex micelles the equilibrium between micellar and polymer species is a function of the salt concentration. In this study we are therefore interested in a limiting salt concentration below which, for given overall polymer concentration, micelles form; by analogy this concentration will be referred to as the critical micellization ionic strength (CMI).

The micellar system in this study consists of three components: a homopolymer, a diblock copolymer and lysozyme. The addition of salt may affect the equilibrium between incorporated and free lysozyme, because the charge density of most protein molecules is relatively low in comparison to the charge density of the polyelectrolytes, i.e., the attraction between the positively charged homopolymers and negatively diblock copolymers is expected to be stronger than the attraction between the negatively charged diblock copolymers and positively charged lysozyme molecules. From small angle neutron scattering (SANS) on lipase-filled micelles a decrease in core volume has been observed when the salt concentration was increased. Assuming this decrease to be caused solely by a gradual release of the protein molecules, we could estimate that beyond a salt concentration of 0.12 M NaCl, all the protein molecules were released [17].

In the following, our interest is in structural and thermodynamical aspects of protein uptake in polyelectrolyte complex micelles. The approach involves the following three steps. First "empty" (i.e., protein free) micelles consisting of homopolymer and diblock copolymer only, were studied. The model is designed to closely match the polymers that were used in experiments. The second step is to find a suitable model for the selected protein molecule lysozyme. Lysozyme is modeled as a linear copolymer where each amino acid in the primary sequence is represented by either a polar, an apolar, a negatively or a positively charged (amino acid) segment. The modeling of the empty micelles, as well as that of the molten globule lysozyme was performed in a one-gradient SCF calculation, using spherical geometry. In the third step we probe the free energy landscape associated with bringing a lysozyme molecule from a large distance into the micelle. These calculations call for a two-gradient SCF analysis using a cylindrical coordinate system. For all the systems, our interest is in studying the effect of the salt concentration. We now argue that this information can be obtained even when explicit electrostatic effects are not accounted for.

Consider, for the sake of argument, a pair of oppositely charged polyions, featuring negatively charged units A, and positively charged C units. In charge driven self-assembly it is natural to expect that the attractive interactions (A-C) can be screened by the addition of salt. We now introduce monomeric components, generically named D_1 and E_1, which (in "charge language") have charges corresponding to those of A and C, respectively. In the FH language we obtain attractive (correlation) whenever interactions $\chi_{DE}=\chi_{DC}=\chi_{AE}=\chi_{AC}\ll 0$. In the presence of D_1 and E_1 a process which may be referred to as screening of A-C interactions occurs. Instead of making many A-C contacts, a sufficient concentration of "salt" (D_1 and E_1) prompts the system to predominantly makes A-E and C-D contacts that are not productive in the sense that they give a driving force for self-assembly. Hence, the addition of D_1 and E_1 eventually causes the micelles to disintegrate, similarly as is known to occur upon the adding salt to the experimental systems.

For polyelectrolyte complex micelles one often invokes the "entropy release" (of the 1:1 electrolyte) argument to rationalize their formation. Screening of interactions, as discussed above, is a very similar entropic effect. Only when these ions cannot gain enough translational entropy (i.e., at high salt concentrations) they will not contribute to the formation of micelles, in other cases they apparently support the formation of micelles.

The protein insertion in polyelectrolyte complex micelles discussed below comes from the correlation attraction, but as stated already, our method cannot treat the ionic interactions in the system explicitly. We nevertheless keep small ions as a component in order to mimic the screening of the electrostatic attraction. It therefore makes sense to continue using "electrostatic language" to describe the homopolymers, diblock copolymers and the small ions. This will make the following discussion more transparent.

In this paper we like to mimic an experimental system on which one diblock copolyelectrolyte, a homopolyelectrolyte, lysozyme, and 1:1 electrolyte are present (see Fig. 1). Before we will give information on the model that is used, we will first mention important thermodynamic quantities that are used to evaluate the micelles seen in an SCF analysis. This is followed by a short introduction to the SCF machinery.

II. THEORETICAL PRELIMINARIES

Classical thermodynamics fails to give detailed information on the formation of association colloids. In a macro-

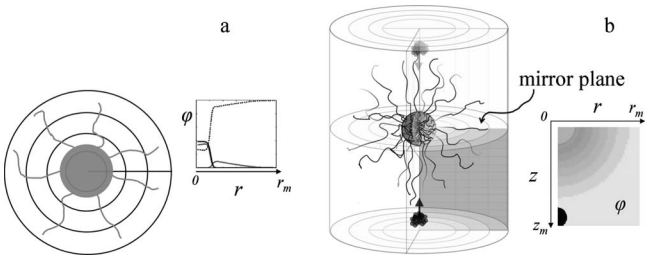

FIG. 2. Schematic representation of (a) one-gradient spherical coordinate system $(r=1,\ldots,r_m)$ and (b) two-gradient cylindrical coordinate system $(z,r)=(1,\ldots,z_m,1,\ldots,r_m)$. Both in (a) and (b) schematic interpretation of the way the molecules are organized is shown pictorially as well as in terms of a radial volume fraction (a) or equal density gray scale plot (b). The mirror plane is indicated by an arrow.

scopically homogeneous system the internal energy U is a function of entropy (S), volume (V), and $\{n\}$ only, $\{n\}$ is the number of molecules of various types in the system. There is no external parameter linked to, e.g., the number of micelles in the system. On the level of the classical thermodynamics this number is irrelevant. Even if there would be a hidden parameter representing this number, say $\mathcal{N}$, its corresponding intensive variable must necessarily remain zero, $\varepsilon=0$; in words, there is no excess free energy associated with the formation of micelles.

The approach to study association colloids in a molecular (SCF) model is fundamentally different. At the basis of the SCF analysis one has to choose the geometry of the system (below we make use of a one-gradient spherical coordinate system and a two-gradient cylindrical one, see Fig. 2) and one must specify the number of molecules in this volume. The micelle that is constructed in this geometry is pinned with its center of mass to a well-defined coordinate. This occurs without the need to restrict the translational degrees of individual molecules; only the translational entropy of the micelle as a whole is ignored by this pinning. Hence, instead of a hidden parameter $\mathcal{N}$, we have (typically) exactly one (explicit) micelle in the system. The associated thermodynamic potential for this micelle, which can be accurately evaluated in the SCF calculation, is given by ϵ_m and differs from ε because the former has no translational degrees of freedom. The difference between the two can thus be seen as the entropy that is lost in the SCF pinning procedure,

$$\varepsilon - \varepsilon_m = k_B T \ln \phi_m. \tag{1}$$

Here $-k_B \ln \phi_m$ is (in dilute solutions) the translational entropy of the micelle (k_B is the Boltzmann constant), while ϕ_m is the volume fraction of micelles in the system. From this equation we can interpret ε as the (excess) chemical potential associated to the presence of micelles. Above we already mentioned that this excess chemical potential must be zero (this follows also from the mass action law for self-assembly) and thus the micelle volume fraction $\phi_m = \exp -\varepsilon_m / k_B T$. For this it is evident that for relevant systems $\varepsilon_m > 0$.

The characteristic function in a SCF calculations is the Helmholtz energy, $F=\varepsilon_m+\Sigma_i n_i \mu_i$ is (when the number of molecules is specified) and this follows from the partition function, i.e., $F=-k_B T \ln Q$. Let the system be composed of $i=1,\ldots,I$, linear molecules having segments with ranking numbers $s=1,\ldots,N_i$. These molecules are composed of a limited set of segment types referred to by X or Y, where, e.g., $X=A,B,C,\ldots$. It is convenient to define chain architecture parameters $\delta_{i,s}^X$. These quantities assume the value unity when segment s of molecule i is of type X and are zero otherwise. The set of $\delta_{i,s}^X$ completely specifies the molecules in terms of its composition.

Here we use the SCF model making use of the discretization scheme of Scheutjens and Fleer [18,19]. In this approach both the macromolecules are assumed to be composed of a discrete set of segments and the space is represented by a lattice, that is, a discrete set of coordinates. The segments and lattice sites match, which means that on each site exactly one segment (or monomeric molecules) can be placed. Here we will illustrate the method by focusing on the one-gradient spherical coordinate system, and trust that the extension to the two-gradient cylindrical coordinate system is clear. In this lattice we distinguish spherical lattice layers referred to by $r=1,\ldots,r_m$. In this geometry the number of lattice sites per layer L grows quadratically with the layer r, i.e., $L(r) \propto r^2$. In each layer we will employ a (local) mean-field approximation and focus on the volume fractions $\varphi_X(r) = n_X(r)/L(r)$, where n_X is the number of sites occupied by segments of type X. This approximation thus ignores the exact position of the segments in a layer, but allows for gradients in composition between layers.

Within the mean-field approximation it is impossible to account accurately for the pair interactions (in contrast to simulations). Instead, it is assumed that the segments feel an external potential $u_X(r)$. Because this potential is not fixed, but (as we will see) is a function of the local distributions, we refer to such potential as being self-consistent. For each segment type X we thus have a pair of distribution functions $\{\varphi(r),u(r)\}$. The free energy is formally given by

$$F(\{\varphi\},\{u\},u') = -k_B T \ln Q(\{u\}) - \sum_r L(r) \sum_X u_X(r)\varphi_X(r) + F^{\text{int}}(\{\varphi\}) + \sum_r L(r)u'(r)\left(\sum_X \varphi_X(r) - 1\right), \tag{2}$$

where u' is the Lagrange multiplier originating from the requirement that all lattice sites are occupied, i.e., $\Sigma_X \varphi_X(r)=1$, $\forall r$. The first term of this free energy shows that we can compute the partition function in "potential" space. The second term of Eq. (2) transforms this result back into the experimentally relevant "concentration" space. The interactions that are present in the system must be (re)added, hence the interaction term F^{int}. This free energy functional need to be at an extreme with respect to its variables; in fact we need to look for saddle points. When for F^{int} a Flory Huggins-like counting of the interactions is implemented, the minimization with respect to the volume fractions gives

$$\frac{\partial F}{\partial \varphi_X(r)} = -L(r)u_X(r) + \frac{\partial F^{\text{int}}}{\partial \varphi_X(r)} + L(r)u'(r) = 0. \tag{3}$$

Within a Flory-Huggins type interaction free energy, the Bragg-Williams approximation is used. Flory-Huggins inter-

action χ parameters give the strength of the interactions (negative for attraction and positive for repulsion),

$$\frac{1}{k_BT}\frac{\partial F^{\text{int}}}{\partial \varphi_X(r)} = L(r)\sum_Y \chi_{XY}(\langle \varphi_Y(r)\rangle - \varphi_Y^b), \tag{4}$$

where φ_Y^b is the volume fraction of segments of type Y in the bulk (far from the micelle where no volume fraction gradients are present, i.e., near $r=r_m$). The angular brackets denote a three-layer average,

$$\langle \varphi(r)\rangle = \lambda(r,r-1)\varphi(r-1) + \lambda(r,r)\varphi(r) + \lambda(r,r+1)\varphi(r+1). \tag{5}$$

Obviously, the *a priori* site probabilities λ add up to unity, i.e., $\Sigma_{r'=r-1,r,r+1}\lambda(r,r')=1$. They further must obey an internal balance equation $L(r)\lambda(r,r+1)=L(r+1)\lambda(r+1,r)$. For $r\to\infty$ $\lambda(r,r+1)=\lambda(r,r-1)=\frac{1}{3}$. With Eq. (4) we can compute the segment potentials $u[\varphi]$ from the volume fractions.

Maximization of the free energy F [Eq. (2)] with respect to the segment potentials leads to the complementary equation $\varphi[u]$,

$$\frac{\partial F}{\partial u_X(r)} = \frac{-k_BT\,\partial \ln Q}{\partial u_X(r)} - L(r)\varphi_X(r) = 0. \tag{6}$$

Here the partition function Q may be decomposed into single-chain partition functions q_i: $Q=\Pi_i q^{n_i}/n_i!$, where n_i is the number of molecules of type i in the system. This formal way to compute the volume fraction $\varphi_X(r)$ as given by Eq. (6) is correct for any chain model, even for self-avoiding chains. Above we have mentioned that we are going to account for interactions on the Bragg-Williams level. At this level the exact positions of the segments are lost and therefore the chain model does not necessarily need to be self-avoiding. Following Scheutjens and Fleer we use a freely jointed chain model for which a very efficient computational route is available that implements Eq. (6). In this approach the volume fraction of segment s of molecule i at coordinate r is computed from the combination of two complementary Green's functions, which specify the combined statistical weights of the possible conformations of complementary chain fragments,

$$\varphi_i(r,s) = \frac{n_i}{q_i}\frac{G_i(r,s|1)G_i(r,s|N)}{G_i(r,s)}. \tag{7}$$

In this equation the single-chain partition function $q_i = \Sigma_r L(r)G_i(r,1|N)$ is interpreted as the overall statistical weight to find molecule i in the system. In Eq. (7), $G_i(r,s)$ is the (free) segment weighting factor for segment s, which is given by the Boltzmann equation $G_i(r,s)=\exp-\frac{u_i(r,s)}{k_BT}$. The end-point distribution functions (Green's functions) $G_i(r,s|1)$ and $G_i(r,s|N)$ follow from the free segment distribution functions through two complementary propagator equations,

$$G_i(r,s|1) = G_i(r,s)\langle G_i(r,s-1|1)\rangle, \tag{8}$$

$$G_i(r,s|N) = G_i(r,s)\langle G_i(r,s+1|N)\rangle, \tag{9}$$

which are started by $G_i(r,1|1)=G_i(r,1)$ and $G_i(r,N|N)=G_i(r,N)$, respectively. The angular brackets indicate a similar averaging as in Eq. (5). We note that the segment potentials are found from $u_i(r,s)=\Sigma_X\delta_{i,s}^X u_X(r)$. Similarly,

$$\varphi_X(r) = \sum_i \sum_s \varphi_i(r,s)\delta_{i,s}^X. \tag{10}$$

The volume fractions of all components in the bulk also obey the incompressibility constraint $\Sigma_X\varphi_X^b=1$ and its evaluation is facilitated by using $n_i/q_i=\varphi_i^b/N_i$.

The saddle point of the free energy is found by a numerical procedure which is stopped when its parameters are self-consistent. This means that the same segment potentials both follow from, and determine the volume fractions, and vice versa that the volume fractions both follow from and determine the segment potentials. The numerical procedure is not stopped until all parameters have a numerical accuracy of seven significant digits, while obeying the incompressibility condition 9. Subsequently, the Helmholtz energy is evaluated accurately and from this all other thermodynamical quantities follow. For example, the chemical potentials of all components are evaluated from the volume fractions in the bulk. Hence the grand potential $\varepsilon_m=F-\Sigma_i\mu_i n_i$ is easily computed.

The results of SCF calculations accurately obey the Gibbs-Duhem equation that relates the grand potential to the chemical potential,

$$d\varepsilon_m = -\sum_i g_i d\mu_i, \tag{11}$$

where the aggregation number, g_i, equals

$$g_i = \frac{1}{N_i}\sum_r L(r)[\varphi_i(r) - \varphi_i^b]. \tag{12}$$

The critical micellization concentration (CMC) is identified from the criterion that $\varepsilon_m(g)$ has a maximum value [20,21]; where $\Sigma_i g_i\mu_i$ is minimized; i.e., $\Sigma_i g_i d\mu_i=0$. The volume fraction of micelles and hence the volume available per micelle $V/\mathcal{N}$ (where V is the volume of the system) can be estimated from Eq. (1). It appears useful to introduce a composition variable as the ratio p^c of negative to positive polymer in the system.

$$p^x = \frac{\varphi_{AB}^x N_A}{\varphi_C^x N_C}, \tag{13}$$

where φ is the overall volume ratio (that is, both contributions from associated and nonassociated polymers in the system) and N is the degree of polymerization. In the calculations we have reasonably easy access to the charge ratio in the bulk p^b and to a ratio that exist in micelles p^m. These ratios are very often not the same, that is, the charge ratio in the bulk may differ strongly from that in micelles. Of course below the CMC there are no micelles and $p^c=p^b$. In general however we would have for micellar solutions,

$$p^c = \frac{\varphi_{AB}^b N_A V + \mathcal{N} g_{AB} N_A}{\varphi_C^b N_C V + \mathcal{N} g_C N_C}. \quad (14)$$

One of the complications in using this equation is the appearance of V and $\mathcal{N}$. Although these can be estimated from using 1, we typically avoid using 14.

At the first appearance of micelles (theoretical CMC), the concentration of the micelles is typically very low and hence the overall polymer concentrations still equal the polymer concentrations in the bulk: $p^c \approx p^b$. On the other hand, when the majority of the polymers is in the micelles, that is, well above the CMC, we can ignore the contribution of the polymers in the bulk and

$$p^c \approx p^m = \frac{g_{AB} N_A}{g_C N_C}. \quad (15)$$

The focus of the current study is to compare calculations to experiments. In experimental conditions, we used a typical concentration of polymers of 1 g L^{-1} which implies approximately $\phi \approx 10^{-4}$. As the CMC is much lower, we conclude that most of the material is in micelles. Without mentioning otherwise we shall approximate $p^c \approx p^m$. This approximation is typically good as long as the system is well below the CMI. We say that we have a "balanced" system, or system with balanced charge stoichiometry when $p^c = 1$. Experimentally, such balanced systems can easily be made by choosing the composition accordingly. Hence, below (or near) the CMC we can impose p^b in the bulk but far above the CMC we can impose p^m in the micelles, respectively.

III. MODEL AND PARAMETERS

A. Coordinate systems

Two different coordinate systems were used: (1) a one-gradient spherical and (2) a two-gradient cylindrical one.

The one-gradient system was used for the "empty" micelle, and for the lysozyme globule, respectively. In this one-gradient lattice, there are spherical lattice layers referred to by $r = 1, \ldots, r_m$, where $m = 80$ [see Fig. 2(a)]. In each layer the volume fractions $\varphi_X(r) = n_X(r)/L(r)$ (where n_X is the number of sites occupied by segments of type X) are determined using the mean-field approximation [22–24]. This approximation allows for gradients in segment composition between layers. The micelle that is constructed in this geometry is pinned with its center of mass to $r = 0$. In Fig. 2(a) the coordinate system and the radial volume fraction $\varphi_x(r)$ are illustrated.

The two-gradient system is used to study micelles in the presence of proteins. In this system the pair of coordinates (z, r) is used, where $z = 1, \ldots, z_m$ (where $z_m = 60$) is along the axis of the cylinder and $r = 1, \ldots, r_m$ (where $r_m = 50$) is the radial coordinate [see Fig. 2(b)]. Now $\varphi_x(z, r) = n_x(z, r)/L(r)$ is the local volume fraction at coordinate (z, r) and the volume fractions are presented as equal density contour plots.

In the two-gradient calculations the center of mass of the micelle is at the symmetry plane pinned at $z = 1$, $r = 1$ [see Fig. 2(b)]. As a consequence of this pinning procedure the calculation deals with half a micelle only. By considering the mirror image [as is depicted in Fig. 2(b)], the volume fractions of the various segments of the whole micelle can be determined. In our approach we "push" one lysozymelike object, which has a central amino acid X (see Fig. 3) at position $(z^*, 1)$, into such micelle by lowering the number of z^* in steps. The same happens for the mirror image and hence we obtain information about the simultaneous insertion of two lysozymelike objects into one micelle. A typical density contour plot of the calculated part of the micelle is given in Fig. 2(b). In Fig. 11, however, we will present the mirror images and present a full cross section through the micelle. The plane of this cross section contains the two mentioned pinning positions.

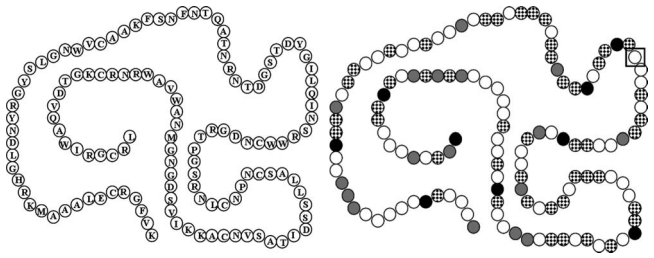

FIG. 3. Sequence of lysozyme and its translation to the segments of our model: N=white, P=checkerboard, K=gray and Z=black. The "translation" of amino acids to segments is given in the text. The □ indicates, the amino acid G (here referred to as X), which was pinned in the two-gradient calculations to a coordinate $(z^*, 1)$.

In SCF calculations the lattice length should be such that the individual segments of the polymers fit in. One of the components in our calculations is a protein. The average size of amino acids is estimated to be around 0.6 nm [25,26]. Therefore we have chosen this value as the lattice length (ℓ) in our calculations. The length also fixes the conversion from volume fractions to (molar) concentrations. For monomeric species the conversion factor is approximately 10.

The dimensions of the lattice volume are fixed by the value r_m in the spherical coordinate system and the set (r_m, z_m) for the cylindrical one. Typically r_m and z_m values were chosen such that the bulk volume fractions prevailed, but small enough so that the calculation times did not become too high. Also the lattice volume is small enough so that, to a good approximation, the majority of the polymer molecules that are in the calculation volume did assemble in the micelle and a negligible part of it remained in the bulk layers (this facilitates the calculations).

B. Molecules

We encounter up to six different molecular species in our SCF calculations:

(1) The homopolymer which is positively charged (homopolyelectrolyte), mimicking $PDMAEMA_{150}$ [poly(N,N dimethylaminoethyl methacrylate)]. This polymer was modeled as a linear chain, having 150 monomers (C).

(2) The diblock copolymer, mimicking PAA_{42}-$PAAm_{417}$ [poly(acrylic acid)-*block*-poly(acryl amide)] consists of two blocks, a negatively charged block which consisted of 40

monomers (A) and a neutral hydrophilic block (B), containing 400 monomers.

(3) The protein molecule was modeled as a linear polymer (see Fig. 3). Amino acids were defined as monomers being either positively charged K=H, K, and R; negatively charged Z=D and E; polar P=S, T, Y, C, N, and Q; or nonpolar N=G, A, V, L, I, F, M, P, and W (here the letters refer to the commonly used one-letter abbreviations of amino acids, see, e.g., biochemistry textbooks). These monomers were placed in the same amino-acid sequence as in lysozyme. In water this lysozymelike molecule collapses to a sort of molten globule.

(4 and 5) are the small ions Cl^- and Na^+, that are used to control the electrostatic interactions.

(6) is the monomeric solvent mimicking water (W). The characteristic distance between two neighboring monomers in one molecule is set equal to the lattice length ℓ.

C. Interaction parameters

Recently, using SCF theory, a model was proposed to study polyelectrolyte complex micelles [7]. The model featured two (symmetric) diblock copolymer types, A_nB_m and C_nB_m, in a nonselective solvent, i.e., for which the Flory-Huggins (FH) parameters with the solvent χ_{SA}, χ_{SB}, χ_{SC} were near the theta-value, i.e., $\chi \approx 0.5$. Self-assembly was shown to occur when the $\chi_{AC} \ll 0$. It was argued that this attraction between A and C can mimic the electrostatic attraction between two oppositely charged segments as these occur in polyelectrolyte complex micelles. We refer to this as the correlation attraction. The B-block is the corona chain which accumulates as a well-solvated polymer brush is formed around the (less swollen) core forming chains A and C. In this model the two polymers had identical block lengths, which helped the theoretical analysis of self-assembly enormously. However, it was shown (only as an example) that stable micelles also form in a mixture of homopolymer A_{N_A} with diblock copolymer $C_{N_C}B_{N_B}$, where N_A is the length (in number of segments) of block A, etc., and that such micelles have a larger aggregation number than in the binary diblock copolymer system. The reason for this is obvious, as the growth of the micelles is stopped by the crowding of chains in the corona. When there is just one type of diblock copolymer in the system, the number of such corona chains per A-C contact is lower when a homopolymer-diblock copolymer system is used, than in the case of two diblock copolymers.

In the present study we make use of a slightly adjusted parameter set. The reason for using a more detailed set of parameters is to tune the model to the experimental data. It is illustrative to discuss the differences between the "old" and current set of parameters. As starting point for the calculations in this study, old Flory-Huggins parameters were chosen for the current A_{40}-B_{400}, C_{150} system. Specifically, for the correlation attraction parameter between the charged block of the diblock copolymer and the homopolymer $\chi_{AC}=-3$ was chosen. The Flory-Huggins (FH) parameters with the solvent (W) for the different segments are all set to the theta-value $\chi_{WA}=\chi_{WB}=\chi_{WC}=0.5$.

The radial volume fraction profile of a typical micelle obtained by these interaction parameters close to the CMC

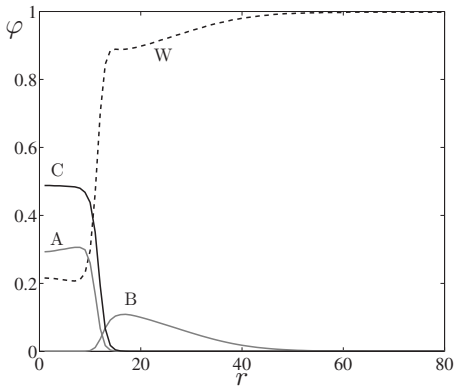

FIG. 4. Radial volume fraction profile of a micelle near the CMC, consisting C_{150} and A_{40}-B_{400} with equal bulk concentrations of φ of solvent (W), homopolymer (C), soluble block (B) and charged block (A) of the diblock copolymer. The FH-interaction parameters are $\chi_{AC}=3$ and $\chi_{WA}=\chi_{WB}=\chi_{WC}=0.5$. These micelles contain approximately 40 diblock copolymers and 20 homopolymers.

while the system is electrostatically balanced, is shown in Fig. 4. As the focus here is on micelles near the CMC it is reasonable to implement the (balancing) constraint $p^c=p^b=1$, that is, the bulk charge concentrations of the two different components are kept the same. In Fig. 4 the radial volume fraction profiles of the different components (A, B, C, and W) are plotted as function of the layer number (r). As expected segment A and C are mainly found in the core of the micelle (layer number 1–12). The corona-forming segment B is found from layer number 12–45. The amount of water W in the core of the micelle is ≈ 0.2, this amount increases from layer number 12–45 and becomes close to unity outside the micelle. The core corona interface is rather sharp (a few lattice lengths).

Because of the strong negative χ_{AC} value ($\chi_{AC}=-3$), the system tries to optimize the number of AC contacts (which occurs locally when $\varphi_A=\varphi_C$). However, the compositional asymmetry between the two polymers: linear polymer (C_{150}) versus diblock copolymer (A_{40}-B_{400}), clearly prevents the perfect realization of charge stoichiometry $p^m=1$ in the micelle. In the core, the homopolymer is clearly favored over the diblock copolymer, when the bulk concentrations are chosen such that the ratio between homopolymer and diblock copolymer in the bulk is unity ($p^b=1$). The corona-forming block B hinders the accumulation of diblock copolymers and the A block being much shorted than the C chain also opposes balanced micelles $p^m=1$. For the current parameter set $p^m<1$ persists also at higher micelle concentration and we decided to restore the balance somewhat by choosing $\varphi_{WC}=0.2$. Improving the solvent quality of C reduces the partitioning of the homopolymer in the micelles. It further increases the overall water content of the micelle, and indirectly, reduces the driving force for micelle formation.

Using $\chi_{WC}=0.2$, micelles were formed that were significantly closer to "charge stoichiometry" than the micelle shown in Fig. 4. The aggregation number of these micelles was still rather high in comparison to the experimental data. To decrease the aggregation numbers, the interaction be-

TABLE I. Flory-Huggins interaction parameters.

χ	W	N, X	C, K, Na^+	A, Z, Cl^-	B, P
W	0	4	0.2	0.5	0.45
N, X	4	0	2.5	2.5	2.5
C, K, Na^+	0.2	2.5	0	−3	0.5
A, Z, Cl^-	0.5	2.5	−3	0	0.5
B, P	0.45	2.5	0.5	0.5	0

tween water and the corona-forming block χ_{WB} was slightly reduced to 0.45. The improved solvent quality of the corona block B strengthens the stopping mechanism of the micellar growth. The interactions between the charged segments of the homopolymer and diblock copolymer with the corona-forming block were unchanged with respect to the old parameter set ($\chi_{AB}=\chi_{BC}=0.5$). To reduce the number of different interaction parameter values, the simple ions were given the same interaction parameters as the like-charged segments of the polymers, i.e., with other segments (y) ($\chi_{Ay}=\chi_{Cl^-y}$ and $\chi_{Cy}=\chi_{Na^+y}$). As a result, specific ionic effects are ignored.

As mentioned, the lysozymelike molecule is built up from four different segments: Nonpolar (N), Polar (P), positively charged (K), and negatively charged (Z) (see Fig. 3). The charged amino acids were given the same interaction parameters with segments (y) as the like charged polymer segments and simple ions: ($\chi_{Zy}=\chi_{Ay}=\chi_{Cl^-y}$ and $\chi_{Ky}=\chi_{Cy}=\chi_{Na^+y}$). The polar segments were given the same interaction parameters as the corona-forming block ($\chi_{By}=\chi_{Py}$). The nonpolar segments N of the protein globule are very important for the structure. Their strong hydrophobicity leads to strong repulsion between the solvent and these segments which we capture by $\chi_{NW}=4$. As there are many hydrophobic segments we observe a collapse of the linear chain to a single proteinlike globule. The Flory-Huggins interaction parameter between the polar and charged segments with the nonpolar segments is set to $\chi_{NK}=\chi_{NZ}=\chi_{NP}=2.5$. The relatively good solvent quality for P ($\chi_{WP}=0.45$), causes these water-soluble segments to be mainly found at the surface of the molten globule.

The current Flory-Huggins interaction parameters are collected in Table I. In this table it can be seen that no more than five different groups of segments have been defined: solvent (W), nonpolar (N), positively charged (C, K, and Na^+), negatively charged (A, Z, and Cl^-), and water soluble (B and P).

IV. RESULTS AND DISCUSSION

A. One-gradient results

In Fig. 4 the volume fraction profiles for a micelle near the CMC with constraint $p^b=1$ was shown. However, comparison of predictions with experiments calls for micelles that exist at much higher concentrations. More specifically, in corresponding experiments we work at polymer concentrations of approximately 1 g L^{-1}. Assuming that most polymers are in the micelles, this leads to a micelle volume fraction $\varphi_m \approx 10^{-4}$. Using Eq. (1), we find that we should focus on micelles with a grand potential $\varepsilon_m \approx 9.2\ k_BT$. It will be clear that under these conditions and for an asymmetric system, e.g., a homopolymer and a diblock copolymer, the ratio between the polymers in the micelle p^m is very different from that in the bulk p^b [Eq. (13)], and the approximation $p^c \approx p^m$ may be more appropriate. Because of the asymmetry between the charged blocks, we cannot simply impose $p^m=1$. Hence, we need an appropriate strategy to compute relevant micelle compositions. This strategy is explained further on; anticipating results, we will argue that $p^c=p^m=0.85$ corresponds to a most likely composition. We will first show a typical radial volume fraction profile (in Fig. 5) for such a system and then discuss its thermodynamic stability in Fig. 6. In both figures we used a salt concentration of $\varphi_{salt}=0.001$.

In Fig. 5 the radial volume fraction distribution of the different segments for the "optimal" micelle ($p^c=0.85$ is imposed, the volume fraction of micelles is $\varphi_m=10^{-4}$ and the ionic strength is $\varphi_{salt}=10^{-3}$), with the interaction parameters of Table I are presented. It can be seen that both the volume fraction of the interacting part of the diblock copolymer (A) and the homopolymer (C) are maximal in the core of the micelle. The volume fraction of the homopolymer (≈ 0.39) is still higher than the volume fraction of the diblock copolymer (≈ 0.35), but the ratio between these volume fractions is much closer to unity than in Fig. 4. Outside the core the highest volume fraction of the soluble block of the diblock copolymer (B) is found.

From these volume fractions one can determine the radius of gyration R_g of the core and the corona by taking the first moment,

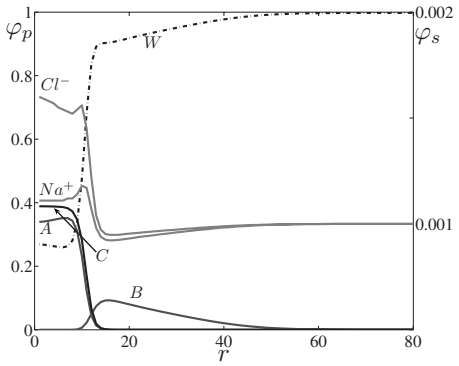

FIG. 5. Radial volume fraction φ_p of water (W), homopolymer (C), soluble diblock copolymer (B), and charged diblock copolymer (A) (left y axis) and radial volume fraction φ_s of Cl^- and Na^+ (right y axis) as a function of the layer number r, $\varphi^b_{salt}=0.001$. Data presented are for: $p^c=p^m=0.85$ (see Fig. 7), volume fraction of micelles is $\varphi_m=10^{-4}$.

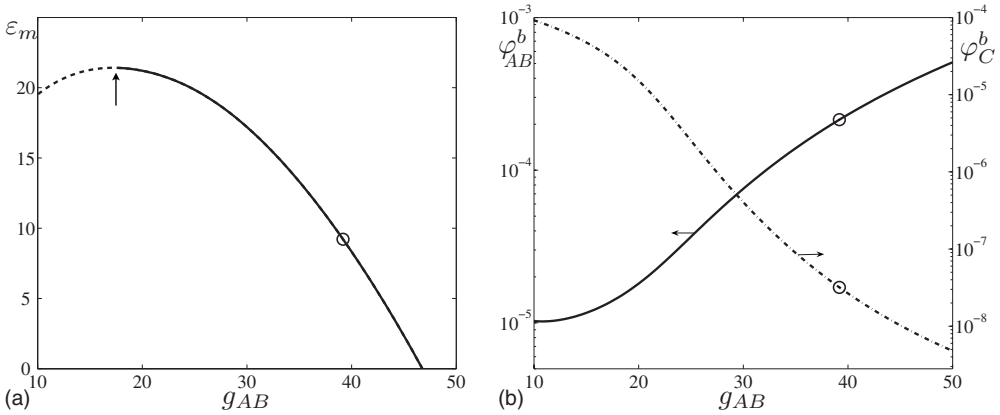

FIG. 6. (a) Grand potential ε_m in units of k_BT as a function of the aggregation number of copolymers (g_{AB}) and (b) φ^b_C (dashed line) and φ^b_{AB} (solid line) on a logarithmic scale as a function of the aggregation number (g_{AB}). The circles in both figures point to the micellar system for which the radial profiles were shown in Fig. 5. Here the constraint $p^c=p^m=0.85$ is used and $\varphi_{salt}=0.001$ and $\varphi_m=10^{-4}$. Micelles indicated by the dashed line [left of the arrow in (a)] are unstable.

$$R_g = \sqrt{\frac{\sum_r L(r) r^2 [\varphi(r) - \varphi^b]}{\sum_r L(r)[\varphi(r) - \varphi^b]}}, \tag{16}$$

where $\varphi(r)$ and φ^b are the volume fractions at layer r and in the bulk, respectively. As an estimation of the $R_{g_{core}}$ we used Eq. (16) with $\varphi=\varphi_C$; taking into account the lattice length of 0.6 nm, this results in $R_{g_{core}} \approx 5.4$ nm. Since for a sphere with homogeneous density $R_g^2=\frac{3}{5}R^2$, the core radius is estimated by $R_{core} \approx 7$ nm. We may estimate the hydrodynamic radius R^h of the micelle by using the volume fraction of the terminal B segment of the copolymer in Eq. (16). By doing so we find $R^h \sim R_{g_{micelle}} \approx 26$ nm. For the experimental micelles approximately the same radii are found, namely $R_{core} \approx 11$ nm and $R_h \approx 27$ nm [16].

The volume fractions of water (W) and small ions (Cl^- and Na^+) are also shown in Fig. 5. The volume fraction of water is minimal in the core of the micelle and increases in the outward direction; outside the micelle the volume fraction of water is unity as expected. Please note that the y axis of the small ions Cl^- and Na^+ is found on the right-hand side of the diagram. The amount of Cl^- ions in the core is a bit higher than that of Na^+ ions. This is because Cl^- is attracted to the (positively charged) homopolymer, which is slightly in excess in the core. This indicates that the micelle tends to approach charge neutrality. At the core-corona interface both volume fractions of the ions have a small maximum. This indicates adsorption, and is a consequence (induced by the chosen parameter set) of the presence of an interfacial tension between the core and the corona. By accumulating at the core-corona interface the ions reduce the unfavorable core-corona contacts and lower the interfacial tension.

Proper stability curves for micelles feature a grand potential (ε_m) as function of the aggregation number (g_{AB}) with a maximum. For thermodynamic stability, however, we must require that $\varepsilon_m > 0$ but also $\frac{\partial \varepsilon_m}{\partial g_{AB}} < 0$. In Fig. 6(a) it can be seen (arrow) that, insisting on the constraint $p^c=0.85$ even near the CMC, the smallest stable micelles have $g_{AB} \approx 17$ where the corresponding grand potential is 22 k_BT. This implies that the volume fraction of micelles near the CMC is very low: $\phi_m \approx 2 \times 10^{-10}$. Such low concentrations are difficult to study by experimental techniques. In our experiments the micellar concentration is much higher, namely, 1 g L^{-1}, and the value of $\varepsilon_m \approx 9.2$ k_BT, which corresponds to a volume fraction of micelles of $\varphi=10^{-4}$, is experimentally more relevant. In Fig. 6(a) the system with this grand potential is indicated with a circle, the aggregation number of this micelle is about twice the value of the smallest stable micelle, namely, $g_{AB} \approx 39$.

The corresponding volume fractions of the homopolymer φ^b_C and diblock copolymer φ^b_{AB} in the bulk as function of the aggregation number (g_{AB}) are presented in Fig. 6(b), on a logarithmic scale. Here again, the selected micelle (shown in Fig. 5) is also indicated by a circle. In this figure it can directly be seen that close to the CMC ($g_{AB} \approx 17$), $\varphi^b_{AB} \approx \varphi^b_C$, so that p^b is close to unity, as was imposed as a constraint in Fig. 4. An increase in aggregation number induces an asymmetry in the bulk: φ^b_C decreases much more than φ^b_{AB}. This indicates that the composition of the micelle and the bulk strongly depend on the micelle concentration. For the micelle of our interest, indicated by $\circ$ ($\varphi_m=10^{-4}$, $p^m=0.85$, and $\varphi_{salt}=0.001$), in the bulk $\varphi^b_{AB} \gg \varphi^b_C$ and $p^b \approx 10^4$.

When the number of contacts between the oppositely charged groups of the polymers (AC) is maximal, in the ideal case, the ratio between the number of homopolymers (C_{150}) and diblock copolymers (A_{40}-B_{400}) should be 4:15. However, since we are dealing with an asymmetric system this ratio may be hard to get, as was already discussed in Fig. 5. From Fig. 6 we calculated that for micelles with $\varphi=10^{-4}$, the aggregation numbers were $g_{AB} \approx 39$ and $g_C \approx 12$. These calculations were performed at fixed homopolymer to diblock copolymer ratio in the system. We still need to justify this particular choice. In Fig. 7(a) it is presented how this ratio was determined.

The key idea is to focus on systems with a *fixed* volume fraction of micelles. For this we have chosen the experimental value, i.e., $\varphi_m=10^{-4}$. This concentration of micelles can occur for a range of g_{AB} and g_C values, each representing

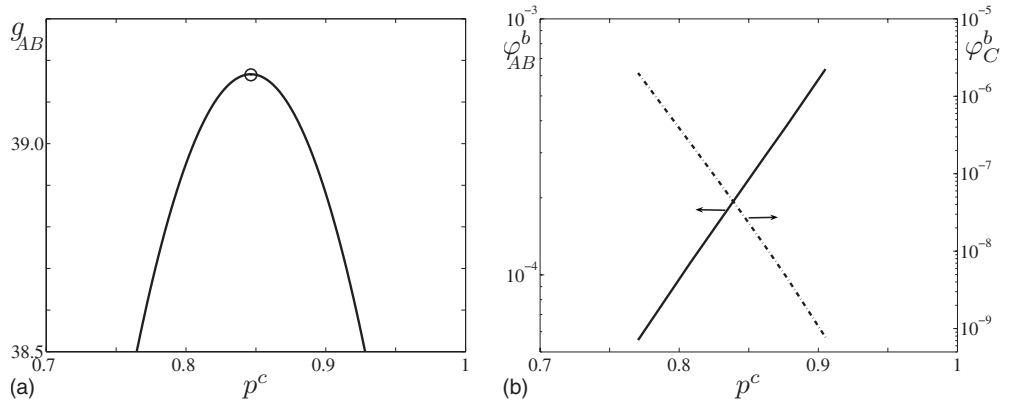

FIG. 7. (a) Aggregation number (g_{AB}) as function of the diblock copolymer/homopolymer ratio (p^c) and (b) φ^b_C (dashed line) and φ^b_{AB} (solid line) on a logarithmic scale as function of p^c, $\varphi_{salt}=0.001$. In all calculations the volume fraction of micelles is fixed to $\varphi_m=10^{-4}$.

micelles at a different p^c value. There are various ways to present the results. We choose to show the aggregation number of diblock copolymers (g_{AB}) as function of the ratio p^c between the diblock copolymer and homopolymer [see Eq. (15)] in the system in Fig. 7. We emphasize that we are far from the CMC and thus $p^c \approx p^m$. In Fig. 7(a) a maximum is found for the aggregation number (g_{AB}) as a function of p^c. This maximum is interpreted as the micelle with optimal (preferred) composition [12]. The maximum is found at $p^c=0.85$. The motivation for this choice is that for optimal conditions the aggregation number should be larger than for suboptimal conditions (at fixed micelle concentration). The corresponding ratio between homopolymer and diblock copolymer was used in al subsequent calculations, hence in Figs. 5 and 6, but also for later figures.

Results presented in Fig. 7(a) have an experimental counterpart, even though in experiments it is virtually impossible to vary the composition in the system at fixed micelle concentration. Nevertheless, a maximum as function of the ratio between homopolymer and diblock copolymer is indeed observed in experiments. The experimental technique of choice to study the polyelectrolyte complex micelle formation is a light scattering (LS) titration. During a LS-titration measurement, a solution containing polyelectrolytes with given charge is titrated to a solution containing oppositely charged macromolecules. After every titration step the light scattering intensity is measured and presented as function of the composition F^- ($F^-=\frac{p^c}{p^c+1}\approx\frac{p^m}{p^m+1}$). Typically, intensity versus composition [$I(F^-)$] plots have a maximum at the optimal micellar composition. Because the mass of the scattering objects is maximal at this composition, it is assumed that the polyelectrolyte complex micelles have the optimal ratio between the oppositely charged macromolecules. Typically, one expects that, experimentally, $p^m \approx 1$, but small deviations have been observed [27]. Our results show that $p^m < 1$ is indeed probable.

For all the systems with fixed micelle concentration, not only the grand potential, but also the two bulk volume fractions are known. Corresponding to the data of Fig. 7(a), φ^b_{AB} and φ^b_C versus g_{AC} are presented in Fig. 7(b) on log-lin coordinates. At $p^c=0.85$ the volume fraction of diblock copolymer is approximately 10^4 times higher than the concentration of homopolymers in the bulk. Again, the large value of p^b is expected because of the molecular asymmetry in the system. The diblock copolymer is hindered to accumulate in the micelle by its B block. In other words, it is hard to increase the amount of diblock copolymers to levels comparable to that of the C polymer to optimize the AC contacts. This simply implies that in order to have $p^m \approx 1$, the concentration of free diblock copolymers in solution must be relatively high (compared to that of the homopolymer). Extrapolating this result to the experimental situation suggests that during a LS titration, the concentration of free diblock copolymers in solution can be much higher than that of the homopolymer. Whether the total amount of copolymer in the bulk becomes so high that one underestimates the amount of (co)polymers in the micelles will depend strongly on the strength of the driving force (e.g., the ionic strength).

From our experiments we gained some information about the disintegration process of the micelles upon the addition of salt. Increasing the salt concentration weakens the electrostatic attraction between the oppositely charged molecules. Light scattering titrations where salt is titrated to the micelles, and SANS measurements at different salt concentrations, revealed that the scattering intensity and aggregation number decrease upon increasing ionic strength. Because the charge density of the protein molecules is lower than the charge density of the polyelectrolytes, a two-step disintegration process has been proposed. First, the protein molecules are released (at $\approx$0.12 M NaCl) and then the micelles disintegrate (at $\approx$0.5 M NaCl). It was therefore chosen to try to find additional proof for the salt-induced release.

In Fig. 8 a few characteristics of the polymer micelles as function of the salt concentration are shown. Again, the ratio between homopolymer and diblock copolymer was fixed at the optimal value, i.e., $p^c=0.85$. Obviously, insisting on $p^c=0.85$ is an approximation; for each ionic strength, a different optimal composition may exist. Hence, by fixing $p^c=0.85$ we ignore such compositional drift; however, it is expected to be significant only around the CMI. The choice to fix p^c is a pragmatic one, as it keeps the computational efforts within reasonable bounds. The salt concentration was varied per calculation and the aggregation numbers of the micelles were determined at fixed micelle concentration ($\varphi_m=10^{-4}$). In Fig. 8(a) one can see that g_{AB}, and thus g_C,

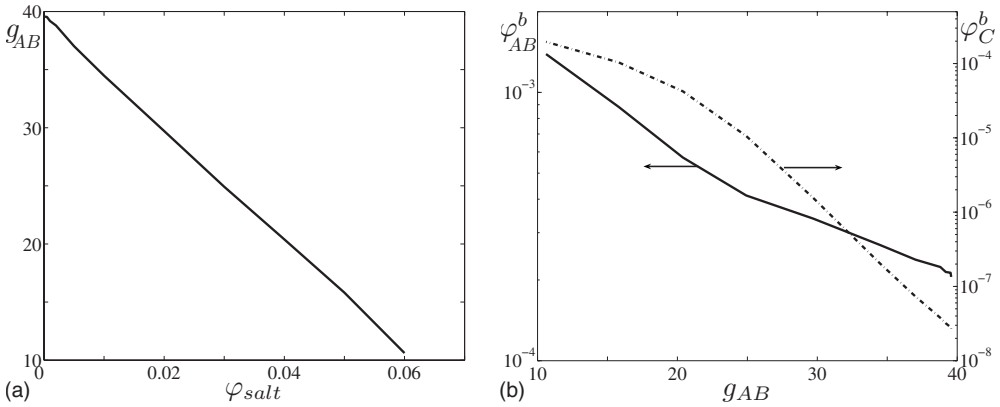

FIG. 8. (a) Aggregation number (g_{AB}) as a function of the salt concentration and (b) dashed line is φ^b_C and solid line is φ^b_{AB} on a logarithmic scale as function of the aggregation number. The micelle concentration was $\varphi_m=10^{-4}$ and the calculations were performed at $p^c=0.85$.

decreases (p_m is constant) linearly as function of the salt concentration, which was also found in experiments [17]. Another consequence is that the CMC increases with increasing ionic strength (result not shown). With increasing ionic strength also the maximum of $\varepsilon_m(g_{AB})$ decreases gradually. At some threshold ionic strength it appears that the maximum of $\varepsilon_m(g_{AB})$ drops below our selected value of $\varepsilon_m=9.2\ k_BT$ (where $\varphi_m=10^{-4}$). We concluded that for this polymer concentration we have reached the critical ionic strength, i.e., the CMI. A further increase of the ionic strength will only give micelles in the system if the polymer concentration is raised. In other words, we have reached a condition where the micelles rather suddenly cease to form. For our selected p^m, the highest salt concentration where stable micelles still exist is $\varphi_{salt}\approx 0.06$. Under these conditions, the micelles have a very low aggregation number; it is only $\frac{1}{4}$ of that at the low ionic strength cases.

In Fig. 8(b) the corresponding bulk concentrations of the homopolymer and diblock copolymer are presented as function of the aggregation number g_{AB}. In this diagram it is seen that the bulk concentrations are a very strong function of aggregation number and hence of the ionic strength. With decreasing driving force (increasing ionic strength) the concentration of the homopolymer can increase by several orders of magnitude. At the same time the copolymer concentration increases by just a factor of 10. Hence, p^b goes from a very small value toward unity. Indeed, at low aggregation numbers i.e., at high ionic strength, the concentration of diblock copolymers and homopolymers in the bulk is almost the same and approaches the overall concentration of polymers in the system. This is indicative of approaching the CMC, or more precisely, the CMI, the salt concentration above which no micelles are detected [16,17].

B. Protein, "lysozyme"

The lysozyme molten globule was placed in a one-gradient coordinate system and the radial volume distributions of the different monomers were calculated. Figure 9 presents the volume fractions φ of the different segments of the protein molecule from layer 1–8. These profiles are typical for a molten globule. In this figure one can see that the volume fraction of the nonpolar segments, N, is highest in the center of the molecule. The water-soluble segments (P, K, and Z) are found in a broad interfacial zone of the proteinlike object. In the sequence of lysozyme $\#Z\neq\#K\neq\#P$, therefore the integrated values of the volume fraction distributions of these segments are different. The amount of water in the center of the object is very low (as expected), due to the choice $\chi_{WN}=4$, and increases when the number of nonpolar segments decreases, i.e., at larger r values.

From Fig. 9, the size of the lysozymelike molecule can be estimated. Using Eq. (16), the radius of gyration of the protein molecule was calculated: 2.1 nm. Assuming a homogeneous sphere one can infer a hydrodynamic radius around 2.7 nm; the hydrodynamic radius for lysozyme reported in literature is 2.1 nm [28].

Due to the discrete nature of the lattice with a cell size (ℓ) of 0.6 nm (corresponding to the segment size), we loose information about the protein globule at length scales smaller than ℓ. Hence, the SCF model is a rather rough way to account for compact globular proteins. Nevertheless, the modeling captures the nature of protein as unimolecular micelles in a reasonable way. The hydrophobic segments and hydrophilic segments show significant overlap of their distribu-

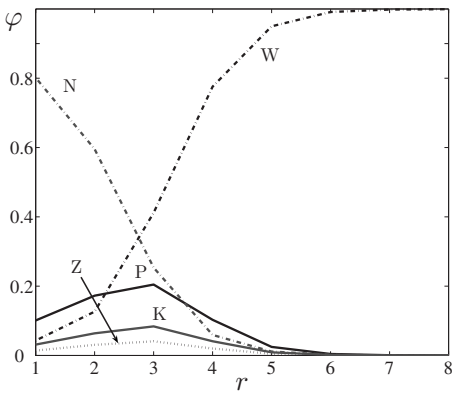

FIG. 9. Radial volume fraction φ of water (W), nonpolar segments (N), polar segments (P), negatively charged segments (Z) and the positively charged segments K of the lysozymelike object as a function of the layer number r.

tions. This must be attributed to the coupling of the primary amino-acid sequence to the overall globule topology.

C. Protein insertion in the polyelectrolyte complex micelle

In this section we will consider the interaction between polymer micelles and proteinlike molecules, modeled in a two-gradient coordinate system. In the absence of the proteinlike molecule, the structure of the micelle in the cylindrical coordinate system is essential identical to that of the spherical coordinate system. Also, the grand potential and the bulk concentrations of its constituents match in both coordinate systems. So, the results obtained from the spherical coordinate system can directly be used to select relevant situations in the computationally challenging cylindrical coordinate system. Again, we will focus on the optimal micelle system, i.e., the micelle with $p^c=0.85$ that exists at a micelle concentration $\varphi_m=10^{-4}$ suspended in a salt concentration of $\varphi_{salt}=10^{-3}$.

As explained in the parameter section, one proteinlike object and half of the micelle were placed inside a two-gradient coordinate system (see Fig. 2) (the other half—its mirror image—is present on the other side of the boundary). One of the nonpolar segments, somewhere in the middle of lysozymelike molecule was pinned (segment X, in Table I and indicated by □ in Fig. 3) to a specified coordinate $(z^*,1)$ and the center of mass of the micelle is in all cases at (1,1). For each specified position z^* of the protein molecule, we can compute the relevant thermodynamic potential

$$F^{po}(z^*) = F - \sum_i \mu_i n_i, \tag{17}$$

where F is the system's Helmholtz energy and the summation over i runs over all mobile components, that includes the two polymers (homopolymer and copolymer), the ions and water. It excludes the proteinlike object itself because we have fixed this molecule to be with segment X at z^*. The partial open free energy F^{po} thus includes both the grand potential ε_m (more precisely: half the grand potential) of the micelles (because the other half is outside the volume) as well as the chemical potential of the proteinlike molecule. Our main interest is in F^{po} as a function of z^*. Systematic variation of the z^* coordinate leads to the free energy of interaction (potential of mean force) of a single protein-micelle pair, $\Delta F(z^*)$,

$$\Delta F(z^*) = F(z^*) - F(\infty), \tag{18}$$

which is presented in Fig. 10. During the calculations the aggregation numbers of diblock copolymer $g_{AB}=39$ and homopolymer $g_{AB}=12$ were effectively kept constant, and the salt concentration was fixed to $\varphi_{salt}=0.001$ as well. In Fig. 11 we present the volume fraction distributions as contour plots through a cross section of the micellar systems, where the protein was pinned at four different positions (a–d in Fig. 10). Since in these viewgraphs cross sections through the whole micelle are presented, there are two proteinlike objects seen in these figures (both the protein and its mirror image).

When the proteinlike molecule is outside of the micelle, (or in the periphery of the corona), the free energy of interaction is to good approximation constant and close to zero $(z^*=20-55)$. The reason for the absence of a repulsive force in the periphery of the corona is that the volume fraction of

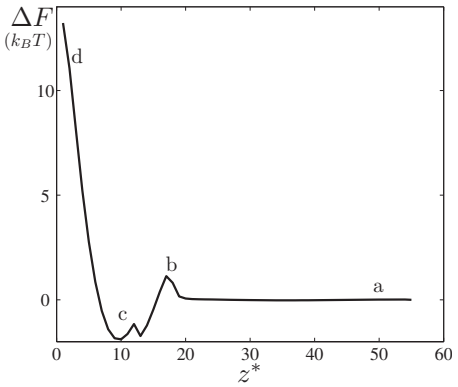

FIG. 10. The free energy of interaction (in units of k_BT) of a micellar system interacting with a lysozymelike molecule pinned at z^* minus that when the lysozymelike molecule is in the bulk $(z^*=\infty)$, ΔF, as function of the pinning position (z^*). In these calculations the ratio between homopolymer and diblock copolymer in the micelles was kept fixed to $p^c=0.85$, $\varphi_m=10^{-4}$, this means that the aggregation numbers of the micelle were fixed as well. The salt concentration was $\varphi_{salt}=0.001$. The cross section through the whole micelle at position of a–d can be found in Fig. 11.

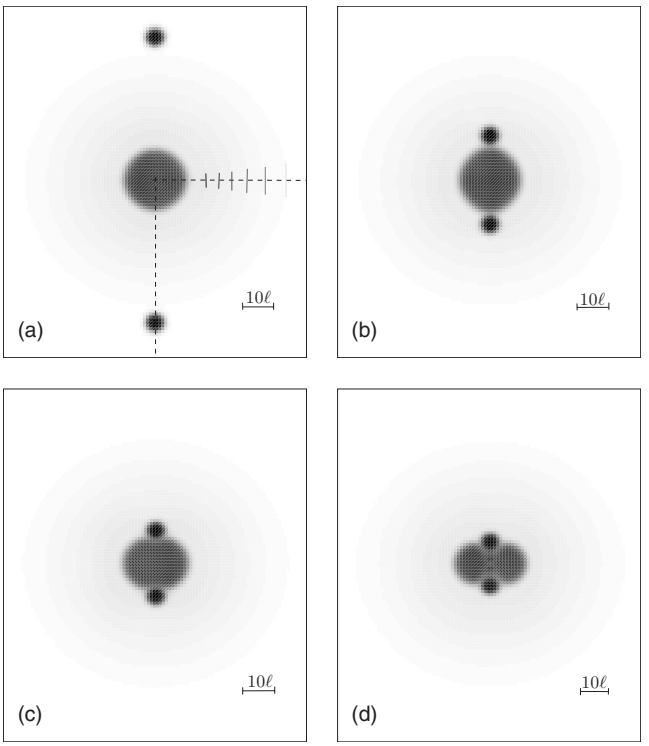

FIG. 11. Two-gradient volume fraction distributions of a micelle with on both sides in the z direction a proteinlike molecule is pinned (a) lysozymes pinned with the X segment at $z^*=|50|$, (b) lysozyme pinned at $z^*=|17|$, (c) lysozymes pinned at $z^*=|10|$ and d) lysozyme pinned at $z^*=|2|$. In figure (a) the volume fraction of diblock copolymer at the respective vertical lines from the core to the outside are: 0.09, 0.075, 0.006, 0.045, 0.03, and 0.015. The scale bar indicates ten lattice sites.

B is very low there. Therefore, there are very few contacts between B and the proteinlike object. Moreover, for $\chi_{WB}=0.45$ the second virial coefficient (v), associated with the corona-solvent interaction, is relatively low ($v=1-2\chi_{WB}=0.1$). As a result the osmotic pressure in the corona remains relatively low. In such situation it is not too expensive to push an object into the outer corona. The free energy of insertion increases when $z^*<20$, and has a maximum when segment X is pinned at position 17. The first idea is that the increase of the free energy is due to the higher concentration of corona chains in this region and thus the insertion against a locally higher osmotic pressure is starting to be significant. To get more detailed insight in what happens we need the distributions of the molecules in the micelle; we will return to this issue once we have discussed these.

Pushing the lysozyme beyond $z^*=17$ into the micelle decreases the free energy. Interestingly, there is a pronounced minimum at position 10, which is at core-corona interface. The irregular change of the free energy of interaction near the minimum proves that there are a number of different contributions to the free energy of interaction which give a subtle change of ΔF (which remain unidentified as yet). Pushing the lysozymelike object further into the core of the micelle results in an unexpected and dramatic increase in free energy. This nontrivial result can more easily be explained once some typical distributions have been discussed.

In Fig. 11 we show the two-gradient volume fraction distributions of the micelle+lysozyme at four different pinning positions: 50, 17, 10, and 2 [Figs. 11(a)–11(d)] as contour plots. In Fig. 11(a), the core (as well as the corona) remains spherical (as expected); the protein molecule is still outside the micelle. Also, the micelle has its unperturbed structure [see Fig. 5; in Fig. 11(a) we also have drawn short vertical lines in the contour plot of which the corresponding volume fractions are given in the legend]. In Fig. 10 we saw that the free energy has a local maximum at layer $z^*=17$, the corresponding contour plot is Fig. 11(b). It can be seen that the core is now slightly elongated in the axial (z) direction. Close inspection of the profiles shows that the elongation of the core is due to a rearrangement of the A segments (charged block of the diblock copolymer) that try to optimize contacts with both the homopolymer (present in the core) and the proteinlike object (both have a same charge, opposite to that of the A block). Such "bridging" leads to a deformed core.

Figure 11(c) shows the contour plot for the case when the lysozyme is pinned at position $z^*=10$, which is in the core-corona interface. From Fig. 10 we know that this is the energetically most favorable position. Now the shape of the core is again close to spherical. Hence, the reduction of the free energy by going from $z^*=17$ to $z^*=10$ is in part the recovery of the elastic deformation of the core. As the interfacial tension is finite, there must be a gain in interfacial free energy accompanied by the adsorption process. In order to estimate this contribution separately we need to evaluate the effective surface tension of the core-corona interface. At present we do not know how to obtain this quantity accurately. To a first approximation, however, we can take the depth of the interaction curve and use the cross-section area of the protein to find an estimate of the surface tension. We then find the fairly reasonable value of $\gamma\approx 1.2$ mN/m.

Note that because we treat the protein molecule as a molten globule (see Fig. 3) it is possible for the molecule to adjust its conformation to the most favorable shape. We acknowledge that our model neglects the two-dimensional (2D) and three-dimensional (3D) structure of the protein molecule. Lysozyme contains several helices and β(-sheets), and is known to have sulfur-bridges between the cysteine residues (see Fig. 3). When it would have been possible to include this structural information into our model, most likely the shape of this proteinlike structure would have been different than the current molten globule. However, this does not necessarily mean that the results of calculations where structural information is included would differ very much from our current results, because the polar and charged amino acids still would mainly be found on the outside of the protein molecule, whereas the nonpolar amino acids would mainly be found at the inside. The interaction with the micelle is expected to be very similar. It should also be realized that in experiments globular proteins have rotational freedom which will also enable them to find the most favorable situation.

In Fig. 10 it can be seen that it is energetically unfavorable to push the lysozyme molecule further into the core of the micelle. In fact, the molecule is forced into the core by the pinning of X. The corresponding two-gradient volume fraction distributions of the micelle and lysozymelike molecule can be found in Fig. 11(d), where $z^*=2$. We, surprisingly, see that the proteinlike object simply refuses to go into the core; instead most of the protein segments remain at the core-corona interface. In this figure one can see that both the morphology of the core as well as the structure of the lysozymelike molecule have changed dramatically when the grafting segment X is put near the center of the core. The core now is flattened in the z direction. This is understood because there is a force acting on the protein toward the center of the core, and as the proteins remain interfacial, the force is balanced by the deformation of the core. Obviously, this nonspherical shape is a very unfavorable situation. How can it be that the proteinlike molecule remains at the core-corona interface while the position of X is near the center? An answer can be found from Fig. 11(d), where in the core two dark spots are seen; these are the pinned segments X. In addition, there is a tether going from $z^*=2$ to the main part of the protein at the core-corona interface (this is more difficult to see, because the tether is smeared). Obviously, it is costly to pull a tether out of the protein, but it is even more costly to bring the entire protein into the core. Both the deformed core and the structural changes of the protein are consistent with the free energy increase that is observed in Fig. 10.

One may argue that the fundamental reason why a proteinlike molecule refuses to go inside the center is that its mirror-image is preventing it to do so. This would be a reasonable explanation if the two lysozyme molecules would indeed repel each other strongly (as they do experimentally under reasonable conditions). Therefore reference calculations were performed in order to quantify the pair interaction between two lysozymelike objects (not shown). From these calculations we learned that these proteinlike objects in fact do not repel each other. The reason is that the long-range

electrostatic effects which in the experimental situation is responsible for the repulsion, is replaced by short-range interactions only. Indeed, in the present model the two lysozyme molecules tend to stick to, rather than repel each other. Hence, an unfavorable pair interaction is not an explanation for the increase in free energy observed in Fig. 10. Apparently, the lysozyme molecule is not wetted by the core components. To deform the shape of the core and to push the homopolymers and diblock copolymers (slightly) away from the center are sufficient to explain the repulsive part of ΔF.

We haste to mention that in the experiments there is no constraining force on the position of one of the amino acids of lysozyme and thus we cannot directly use the free energy curve to compute the equilibrium distribution of the proteins inside the polymer micelle. However, the calculations strongly suggest that proteins will very likely be positioned in the core-corona interface and that there is an energy barrier separating the bound state of the protein (at the core-corona interface) and the unbound one (floating freely in solution).

Let us return to the local maximum found at $z^*=17$. In a mean-field theory one may anticipate that the phenomena that were discussed, i.e., the work against the osmotic pressure (increasing with decreasing z^*) and the elastic deformation of the core (increasing with increasing z^*), may have resulted in a first-order-like transition, with metastable branches in $\Delta F(z^*)$. This does not occur in the present system. Possibly, the reason for this is that the lengths of the polymers that form the micelle were too short for this. We do not exclude, however, that on a mean-field level the transition between bound and unbound states becomes a true transition in the appropriate thermodynamic limit (very long chains). High barriers between bound and unbound states would be of practical interest obviously.

The final question to be addressed is whether, upon increasing the ionic strength, the proteinlike objects are released, and whether (or not) this occurs before the micelles disintegrate. To obtain relevant predictions we have recorded the depth of the free energy of interaction ΔF_{min} as function of the salt concentration. Again we focus on the optimal micelle composition $p^c=0.85$ and keep the micelle volume fraction $\varphi_m=10^{-4}$. Referring to Figs. 8(a) and 8(b), we know that in this system both the aggregation numbers and the bulk concentrations depend on the salt concentration used. To calculate the depth of the free energy $[\Delta F(z^*)]$ as a function of the salt concentration, these features have been implemented as constraints. This means that for a given calculation of $\Delta F(z^*)$ not only the ionic strength, but also the corresponding bulk volume fractions of all polymers were specified. This means that the aggregation numbers could relax to the values reported in Fig. 8, both in the presence and in the absence of the proteinlike molecule.

The first issue is to localize the minimum in the interaction curve. Clearly as the aggregation number changes, it is conceivable that the minimum position of F^* shifts. It was found, however, that the position of the minimum free energy did not change; it remained located at $z^*=10$ for all salt concentration. Using this result, the absolute value of the free energy of interaction $|\Delta F(10)|$, which is the difference in free energy of the micellar system with the proteinlike molecule at $z^*=10$ and at $z^*=\infty$, was determined as function of the salt concentration. The results of these calculations are presented in Fig. 12.

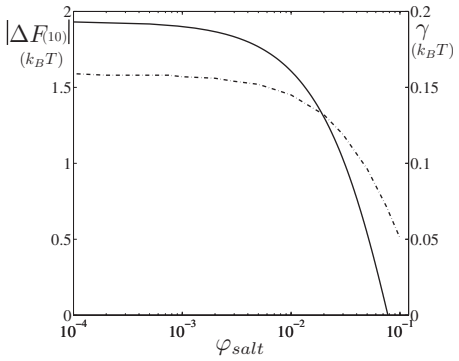

FIG. 12. Absolute value of the free energy of interaction of a lysozymelike object pinned at layer $z^*=10$ (left y axis and solid line), from the center of the micelle, $|\Delta F(10)|$ (in units of k_BT) as a function of the salt concentration. The ionic strength dependence of the bulk concentrations of the homopolymer and diblock copolymer were taken from the results of Fig. 8(b). The volume fraction of micelles is fixed to $\varphi_m=10^{-4}$. Ionic strength dependence of the interfacial tension of a $A_{40}+C_{150}$ complex (right y axis, dashed line) in units k_BT per lattice length squared (ℓ^2).

Based on light- and neutron-scattering measurements as function of the salt concentration it was proposed that first the enzymes are gradually released and then the micelles disintegrate. In Fig. 12 it can be seen that the free energy difference is constant ($\approx 1.9\ k_BT$) up to a salt concentration of 10^{-3}. $|\Delta F(10)|$ decreases with ionic strength when $\varphi_{salt} > 10^{-3}$. At $\varphi_{salt} \approx 0.04$ it is less than k_BT, which indicates that the accumulation of the lysozymelike object must have decreased by a factor of approximately 2.5. This salt concentration is clearly lower than the salt concentration at which the micelles disappear [see Figs. 8(a) and 8(b)]. Hence, this suggests that most of the lysozymelike objects are released before the micelles fall apart. From Figs. 8(a) and 8(b) it became also clear that the aggregation number of the micelles decreases as function of the ionic strength, indicating that, apart from the enzyme release, also homopolymer and diblock copolymers are released. All these results are consistent with the experimental results.

In Fig. 12 we also present the ionic strength dependence of the interfacial tension between water and a macroscopic $A_{40}+C_{150}$ complex phase. Up to an ionic strength of $\approx 2 \times 10^{-2}$ the free energy of interaction $[|\Delta F(10)|]$ and the interfacial tension follow the same trend. Above $\varphi_{salt}=2 \times 10^{-2}$ the decrease in the free energy of interaction is more pronounced than the decrease in the interfacial tension. This correlation between the free energy of interaction and the interfacial tension indicates that the proteinlike object is not wetted by the core-forming phase and therefore has its most favorable conformation in the core-corona interface. The difference in shape, upon comparing the interfacial tension and free energy of interaction at $\varphi_{salt} > 2 \times 10^{-2}$, may be due to the curvature of the micelle, which was not taken into account in our reference calculations, where we just considered a macroscopic (flat) interface. Also, in our reference calcula-

tions we only used the charged block of the diblock copolymer, contributions of the hydrophilic uncharged block B to the interfacial tension in the core-corona interface were thus ignored.

At this stage it is of interest to elaborate shortly on how the calculations compare to corresponding experimental data. We have estimated, from SANS data, the typical aggregation number of the three different components and the amount of water in the core, for a micelle concentration of $\varphi_m \approx 10^{-4}$. The aggregation number of the homopolymer and diblock copolymer in the calculations are 12 and 39, respectively; we pushed 2 lysozyme molecules into these micelles. The experimental micelles contain on average 8 homopolymers, 29 diblock copolymers and 2 lysozyme molecules [16]. Because we deliberately tuned our Flory-Huggins parameters such that these numbers are comparable, we can hardly argue that this is an independent result. However, we can say that the calculations are helpful for giving insight into the experimental system, e.g., in giving structural information.

A key disparity between the experimental data and the model predictions is the amount of water in the core of the micelles. For the experimental micelle the volume fraction of water in the core is estimated to be as high as 0.92; similar volume fractions of water were found for micelles consisting of PAA_{42}-$PAAm_{417}$ and $P2MVP_{209}$ [11]. For the determination of the amount of water in these polyelectrolyte complex micelles, several assumptions have to be made and it is expected that the error is between 10% and 15%. The volume fraction of water in the model micelle is only ≈ 0.30 and thus well outside the uncertainty range of the experiments. In mean-field calculations it is possible to increase the water concentration in the core of the micelles. However, to do so, the strength of the correlation attraction has to be increased to very (unreasonably) high values, while the solvent quality χ_{AW} and $\chi_{CW} \ll 0$. Calculations in this region of parameter space were exceedingly difficult. Here we clearly see a limitation of the Bragg-Williams approximation.

The calculations, nevertheless, give new insights and truly contribute in explaining experimental findings. For the experimental micelle it is for instance known that homopolymer needs to be in excess of like charged protein in order to obtain stable micelles. The above results now may give a clue why this is the case. An explanation may be that the optimal place for a protein is in the core-corona interface. When the protein is in excess, there is not enough interface available for the protein and the structures that are formed have a tendency to disintegrate. In previous work we have found that micelles, where the molar ratio between $PDMAEMA_{150}$ and lysozyme was 13:87, were unstable [4]. Small angle neutron scattering measurements of these structures could not be interpreted using the standard model for a micelle of a (homogeneous) core surrounded by a dilute corona. The preference of proteins to be in the core-corona interface was not considered and may be an explanation for the instability of these micelles and the difficulties in explaining the neutron data.

V. CONCLUSIONS

Self-consistent field modeling is presented which is targeted to identify the main physical characteristics of protein insertion in polyelectrolyte complex micelles. Predictions were, when possible, confronted with experimental data. The attractive interactions between the oppositely charged species are treated on the Flory-Huggins short-range interaction level. Our polyelectrolyte complex micelles consist of homopolymers and diblock copolymers, which means that the system is composition-wise asymmetric. The model allowed flexibility in adjusting the appropriate Flory-Huggins interaction parameters such that the model polyelectrolyte complex micelle truly resembles experimental ones. We have analyzed the charge stoichiometry of the polyelectrolyte complex core, and argue that the optimal charge ratio between diblock and homopolymer is slightly lower than unity, i.e., $p^c = 0.85$.

For most of our results, we fixed our attention to micelles with this optimal ratio and to systems where the micelle concentration and salt concentration were fixed ($\varphi_m = 10^{-4}$ and $\varphi_{salt} = 0.001$) as well. First, a one-gradient spherical coordinate system was used and calculations were performed to characterize the polyelectrolyte complex micelle and the lysozymelike objects separately. Subsequently, the micelle was pinned with its center of mass in a two-gradient cylindrical coordinate system and the lysozymelike object was pushed into the micelle along the cylinder's axis. The free energy as function of the distance to the core has a minimum of $\approx -2\ k_BT$ in the core-corona interface, indicating that this position is favorable in comparison to the bulk or the corona. A dramatic increase in free energy is observed when the lysozymelike object is pushed into the center of the core, showing that the proteinlike molecule strongly prefers the core-corona interface. Importantly, we found that there is a free energy barrier between the bound (protein is at the core-corona interface) and unbound (protein is free in solution) state of the protein. The height of this barrier is determined jointly by the work against the osmotic pressure and the work to deform the core.

The stability of the micelles in terms of ionic strength, was determined and compared to experimental results. First, the aggregation number of the polyelectrolyte complex micelle decreased as function of the ionic strength and at $\varphi_{salt} \approx 0.06$ the critical micelle ionic (CMI) strength is found for micelles where $p^m = p^c = 0.85$ and $\varphi_m = 10^{-4}$. From calculations in the two-gradient coordinate system, where the free energy of the unbound state (protein is outside micelle) is compared to the bound state (protein is at the core-corona interface), it can be derived that the well depth of the protein/micelle potential of mean force decreases strongly upon increasing the ionic strength, well before the themselves micelles vanish. Hence, the proteins loose affinity for the micelles with increasing ionic strength. This salt-induced release was also concluded from the experimental data.

[1] A. Harada and K. Kataoka, Macromolecules **28**, 5294 (1995).
[2] A. V. Kabanov, T. K. Bronich, V. A. Kabanov, K. Yu, and A. Eisenberg, Macromolecules **29**, 6797 (1996).
[3] M. A. Cohen Stuart, N. A. M. Besseling, and R. G. Fokkink, Langmuir **14**, 6846 (1998).
[4] S. Lindhoud, R. de Vries, W. Norde, and M. A. Cohen Stuart, Biomacromolecules **8**, 2219 (2007).
[5] A. Harada and K. Kataoka, Macromolecules **31**, 288 (1998).
[6] A. Harada and K. Kataoka, Langmuir **15**, 4208 (1999).
[7] I. K. Voets and F. A. M. Leermakers, Phys. Rev. E **78**, 061801 (2008).
[8] I. K. Voets, A. de Keizer, P. de Waard, P. M. Frederik, P. H. H. Bomans, H. Schmalz, A. Walther, S. M. King, F. A. M. Leermakers, and M. A. Cohen Stuart, Angew. Chem. Int. Ed. **45**, 6673 (2006).
[9] I. K. Voets, A. de Keizer, M. A. Cohen Stuart, and P. de Waard, Macromolecules **39**, 5952 (2006).
[10] I. K. Voets, A. de Keizer, M. A. Cohen Stuart, J. Justynska, and H. Schlaad, Macromolecules **40**, 2158 (2007).
[11] I. K. Voets, S. van der Burgh, B. Farago, R. Fokkink, D. Kovacevic, T. Hellweg, A. de Keizer, and M. A. Cohen Stuart, Macromolecules **40**, 8476 (2007).
[12] S. van der Burgh, A. de Keizer, and M. A. Cohen Stuart, Langmuir **20**, 1073 (2004).
[13] B. Hofs, I. K. Voets, A. d. Keizer, and M. A. Cohen Stuart, Phys. Chem. Chem. Phys. **8**, 4242 (2006).
[14] D. Wakebayashi, N. Nishiyama, K. Itaka, K. Miyata, Y. Yamasaki, A. Harada, H. Koyama, Y. Nagasaki, and K. Kataoka, Biomacromolecules **5**, 2128 (2004).
[15] D. Wakebayashi, N. Nishiyama, Y. Yamasaki, K. Itaka, N. Kanayama, A. Harada, Y. Nagasaki, and K. Kataoka, J. Controlled Release **95**, 653 (2004).
[16] S. Lindhoud, R. de Vries, R. Schweins, W. Norde, and M. A. Cohen Stuart, Langmuir **25**, 11425 (2009).
[17] S. Lindhoud, R. de Vries, R. Schweins, M. A. Cohen Stuart, and W. Norde, Soft Matter **5**, 242 (2009).
[18] J. Scheutjens and G. J. Fleer, J. Phys. Chem. **83**, 1619 (1979).
[19] J. Scheutjens and G. J. Fleer, J. Phys. Chem. **84**, 178 (1980).
[20] N. A. M. Besseling and M. A. C. Stuart, J. Chem. Phys. **110**, 5432 (1999).
[21] J. Sprakel, F. A. M. Leermakers, M. A. C. Stuart, and N. A. M. Besseling, Phys. Chem. Chem. Phys. **10**, 5308 (2008).
[22] A. B. Jodar-Reyes and F. A. M. Leermakers, J. Phys. Chem. B **110**, 6300 (2006).
[23] F. A. M. Leermakers and J. Scheutjens, J. Colloid Interface Sci. **136**, 231 (1990).
[24] F. A. M. Leermakers, C. M. Wijmans, and G. J. Fleer, Macromolecules **28**, 3434 (1995).
[25] E. B. Zhulina and F. A. M. Leermakers, Biophys. J. **93**, 1452 (2007).
[26] E. B. Zhulina and F. A. M. Leermakers, Biophys. J. **93**, 1421 (2007).
[27] S. van der Burgh, Ph.D. thesis, 2004.
[28] W. Eberstein, Y. Georgalis, and W. Saenger, J. Cryst. Growth **143**, 71 (1994).